Dalton Transactions

PAPER

View Article Online
View Journal | View Issue

Cite this: *Dalton Trans.*, 2015, **44**, 6249

Bright luminescence in lanthanide coordination polymers with tetrafluoroterephthalate as a bridging ligand†

Miriam Sobieray,[a] Jens Gode,[a] Christiane Seidel,[a] Marieke Poß,[b] Claus Feldmann[b] and Uwe Ruschewitz*[a]

Received 5th December 2014,
Accepted 19th February 2015

DOI: 10.1039/c4dt03733b

www.rsc.org/dalton

Ten new coordination polymers of the general compositions $^{2}_{\infty}[Ln^{III}(tfBDC)(NO_3)(DMF)_2]\cdot DMF$ with Ln^{III} = Eu^{3+} (**1**), Gd^{3+} (**2**), Tb^{3+} (**3**), Ho^{3+} (**4**), Tm^{3+} (**5**), $^{2}_{\infty}[Ln^{III}(tfBDC)(CH_3COO)(FA)_3]\cdot 3FA$ with Ln^{III} = Sm^{3+} (**6**), Eu^{3+} (**7**) and $^{2}_{\infty}[Ln^{III}(tfBDC)(NO_3)(DMSO)_2]$ with Ln^{III} = Ho^{3+} (**8**), Er^{3+} (**9**) and Tm^{3+} (**10**) were synthesized and structurally characterized by X-ray single crystal diffraction ($tfBDC^{2-}$ = 2,3,5,6-tetrafluoroterephthalate, DMF = *N*,*N*′-dimethylformamide, FA = formamide, DMSO = dimethyl sulfoxide). **1–5** crystallize in the monoclinic space group *C*2/*c* with *Z* = 8, **6** and **7** in $P\bar{1}$ with *Z* = 2 and **8–10** in *Pbca* with *Z* = 8. All crystal structures contain binuclear lanthanide nodes that are connected by 2,3,5,6-tetrafluoroterephthalates ($tfBDC^{2-}$) to form two-dimensional polymeric structural units. Despite this common structural feature the coordination within these binuclear units is quite different in detail, *e.g.* CN = 9 for **1–7** and CN = 8 for **8–10**. The emission spectra of the europium (**1**, **7**) and terbium (**3**) compounds reveal bright red and green emission in the visible region. The resulting high quantum yields of 53% (**1**) and 67% (**3**) at room temperature show that the replacement of organic ligands with C–H groups by perfluorinated ligands leads to compounds with intense emission, as vibrational quenching is reduced. On the other hand, the influence of the coordinating solvent and additional ligands cannot be neglected, as the replacement of DMF by FA and NO_3^- by CH_3COO^- in **7** leads to a reduced quantum yield of only 10%. Thermoanalytical investigations show that all compounds are stable up to 100–150 °C, before a stepwise release of solvent molecules starts followed by a decomposition of the coordination polymer.

Introduction

Coordination polymers (CPs) and metal organic frameworks (MOFs) have been investigated by many research groups worldwide during the last 15 years. With respect to their applications most of this work has been focused on the porosity of some of these compounds.

But it has already been emphasized that "the field has other opportunities to offer".[1] Therefore a clear trend has been identified in the field of coordination polymers in the last few years, *i.e.* target-oriented synthesis of new ligands for the construction of CPs with new properties and functionalities. In this respect the synthesis of CPs with fluorinated or perfluorinated linkers has attracted increasing attention, as these compounds are supposed to show enhanced adsorption properties[2–6] as well as improved luminescence[7] compared to CPs with typical organic ligands. The latter is due to the fact that C–H quenching, which typically reduces luminescence in organic compounds, is not possible in perfluorinated organics. A linker commonly used in the construction of such coordination polymers is perfluorinated terephthalate.[8] Based on an improved synthesis of this linker, which allows us to synthesize gram quantities of tetrafluoroterephthalic acid with high purity starting from cheaply available chemicals,[9] we have synthesized several coordination polymers with perfluorinated terephthalate as the linker.[10,11] We mainly focused on the luminescence properties of these compounds and showed that coordination polymers of the general composition $^{2}_{\infty}[Ln^{III}(tfBDC)(NO_3)(DMF)_2]\cdot DMF$ (Ln^{3+} = Ce, Pr, Nd, Sm, Dy, Er, Yb; DMF = *N*,*N*′-dimethylformamide) gave intense emissions in the visible region of light for Pr, Sm and Dy with colors ranging from orange, orange-red to warm white.[11]

[a]*Department of Chemistry, University of Cologne, Greinstraße 6, D-50939 Cologne, Germany. E-mail: uwe.ruschewitz@uni-koeln.de*
[b]*Institute of Inorganic Chemistry, Karlsruhe Institute of Technology (KIT), Engesserstraße 15, D-76131 Karlsruhe, Germany*

†Electronic supplementary information (ESI) available: Experimental and simulated powder X-ray diffraction patterns, DTA/TGA diagrams, IR spectra/data, excitation spectra, comparison of excitation and emission spectra, additional figures of crystal structures, and X-ray crystallographic files in CIF format for compounds **1–10**. CCDC 957999–958003 and 1025456–1025460. For ESI and crystallographic data in CIF or other electronic format see DOI: 10.1039/c4dt03733b

Their crystal structures consist of binuclear lanthanide nodes (CN = 9) connected by 2,3,5,6-tetrafluoroterephthalates ($tfBDC^{2-}$) to form two-dimensional polymeric structural units. DMF as well as NO_3^- are also included in the first coordination sphere of the lanthanides. The latter seems to be important for the rigidity of the polymer. In similar compounds of the composition $^2_\infty[(Ln^{III})_2(tfBDC)_3(DEF)_2(EtOH)_2]\cdot 2DEF$ (Ln^{III} = Tb, Gd, Eu, La, Nd; DEF = *N*,*N*′-diethylformamide),[12] which also consist of binuclear lanthanide nodes connected by $tfBDC^{2-}$ ligands to form 2D sheets, no additional anions like nitrates are included in the first coordination sphere of the lanthanide. Red and green emissions have been reported for Eu(III) and Tb(III) compounds.[12] In the following we will present our results on coordination polymers of the composition $^2_\infty[Ln^{III}(tfBDC)(NO_3)(DMF)_2]\cdot DMF$ with Ln^{III} = Eu^{3+} (**1**), Gd^{3+} (**2**), Tb^{3+} (**3**), Ho^{3+} (**4**) and Tm^{3+} (**5**). They are isostructural to the already reported compounds[11] thus completing this series of compounds for all lanthanides with the exception of La^{3+}, Pm^{3+} and Lu^{3+}. As expected red (Eu^{3+}) and green (Tb^{3+}) emissions are found, but high quantum yields of up to 53% for the Eu^{3+} and 67% for the Tb^{3+} compound are remarkable. To investigate the influence of the incorporated DMF molecules and NO_3^- anions on their luminescence properties crystallization from other solvents or with other starting materials (Ln(III) acetates instead of Ln(III) nitrates) was attempted. Thus, five new coordination polymers of the composition $^2_\infty[Ln^{III}(tfBDC)(CH_3COO)(FA)_3]\cdot 3FA$ with Ln^{III} = Sm^{3+} (**6**), Eu^{3+} (**7**) and $^2_\infty[Ln^{III}(tfBDC)(NO_3)(DMSO)_2]$ with Ln^{III} = Ho^{3+} (**8**), Er^{3+} (**9**) and Tm^{3+} (**10**) were obtained (FA = formamide, DMSO = dimethyl sulfoxide).

Results and discussion

By a diffusion controlled crystallization method developed earlier[11] (see the Experimental section) we were able to synthesize single crystals with sizes up to several millimeters of coordination polymers with the general formula $^2_\infty[Ln^{III}(tfBDC)(NO_3)(DMF)_2]\cdot DMF$ with Ln = Ce, Pr, Nd, Sm, Dy, Er, Yb.[11] In this work we have now been able to complete the series with most of the missing members of the lanthanide row, *i.e.* Ln = Eu (**1**), Gd (**2**), Tb (**3**), Ho (**4**) and Tm (**5**). So only compounds with the largest (Ln = La) and the smallest lanthanide (Ln = Lu) as well as with radioactive Pm are still unknown. All compounds crystallize with the same structure type in the space group *C*2/*c* (no. 15) with *Z* = 8. The unit cell volumes decrease with increasing atomic number as expected for lanthanide contraction (Fig. 1).

As the crystal structure of $^2_\infty[Ln^{III}(tfBDC)(NO_3)(DMF)_2]\cdot DMF$ compounds has already been discussed earlier,[11] only a brief description shall be given here taking $^2_\infty[Eu^{III}(tfBDC)(NO_3)(DMF)_2]\cdot DMF$ (**1**) as an example for all other isostructural compounds **1**–**5**. The asymmetric unit of **1** contains one Eu^{3+} cation, one NO_3^- anion and three DMF molecules, all in general positions. However, two crystallographically independent $tfBDC^{2-}$ anions are found. Both are located on symmetry

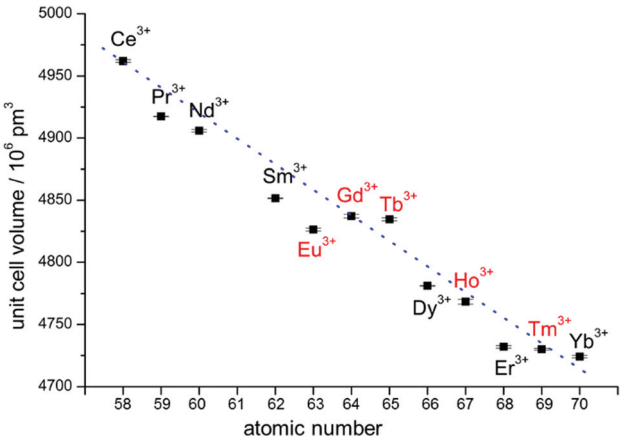

Fig. 1 Unit cell volumes of coordination polymers $^2_\infty[Ln^{III}(tfBDC)(NO_3)(DMF)_2]\cdot DMF$; volumes with black atomic symbols are taken from ref. 11, with red symbols: this work. The blue dotted line is a guide for the eye.

elements (inversion center and two-fold axis, resp.), so a full anion is generated by these symmetry elements. In Fig. 2 the coordination sphere around one Eu^{3+} cation is shown. Eu^{3+} is coordinated by nine oxygen atoms (CN = 9) stemming from three monodentately coordinating carboxylate groups of the $tfBDC^{2-}$ ligand (Eu–O: 238.9(4)–239.7(4) pm), one chelating bidentately coordinating carboxylate group of the $tfBDC^{2-}$ ligand (Eu–O: 249.9(4) and 262.3(3) pm), one chelating bidentately coordinating NO_3^- anion (Eu–O: 250.0(5) and 252.6(4) pm) and two coordinating DMF molecules (Eu–O: 238.7(4) and 239.6(5) pm). The next-nearest distance is Eu–C7 with 291.2(4) pm. The EuO_9 polyhedra are linked by a common edge and bridged by the carboxylate groups of two $tfBDC^{2-}$ ligands to form dimeric units (Fig. S22, ESI†). The Eu–Eu distance within these dimers is 406.67(8) pm. For comparison, in elemental Europium the shortest Eu–Eu distance is 396 pm. In the series of the coordination polymers $^2_\infty[Ln^{III}(tfBDC)(NO_3)(DMF)_2]\cdot DMF$

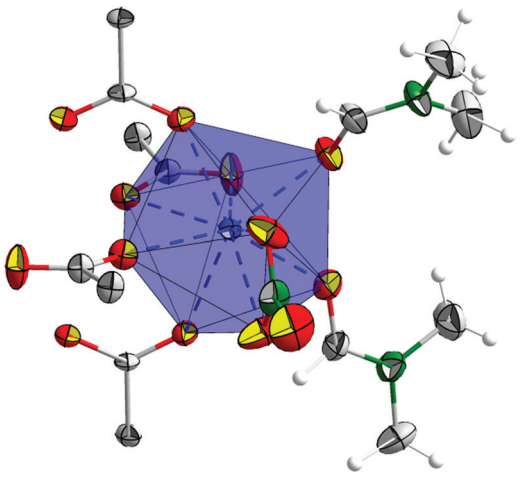

Fig. 2 ORTEP plot (50% probability) of the coordination sphere around Eu^{3+} in $^2_\infty[Eu^{III}(tfBDC)(NO_3)(DMF)_2]\cdot DMF$ (**1**); Eu (blue), O (red), C (light gray), N (green), H (small white spheres); the $tfBDC^{2-}$ ligand is only partly depicted.

the Ln^{III}–Ln^{III} distances decrease with increasing atomic number (Table 3). The same trend is found for Ln^{III}–O distances (Table 3). These dimeric $(EuO_{7/1}O_{2/2})_2$ units are connected *via* $tfBDC^{2-}$ ligands to form sheets with distorted square grids in the (100) plane (Fig. S23, ESI†). One $tfBDC^{2-}$ ligand connects along [010] and the other along [001]. These layers are stacked along [100] in an AB fashion with a translation vector ~1/2 1/2 0, so that the dimers of the next layer are not positioned above the center of the square grids of the layer below, but above their edges. The layers are held together by weak van der Waals forces. Non-coordinated DMF molecules fill the space in-between the layers, but also the space within the square grids so that no pores are found in this coordination polymer.

It has been shown earlier[10] that the benzene rings and carboxylate groups are not coplanar in tetrafluoroterephthalates due to an electrostatic repulsion between the fluorine atoms on the ring and the oxygen atoms of the carboxylate groups as well as due to a decrease in the aromatic character of the carboxylate group due to the electron-withdrawing nature of the fluorine atoms.[23,24] Therefore torsion angles between the benzene rings and the carboxylate groups of 79.0(2)° (2×), 48.1(4)° and 52.1(4)° are found for the two crystallographically independent $tfBDC^{2-}$ ligands in **1**. For symmetry reasons the carboxylate groups themselves are coplanar in $tfBDC^{2-}$ ligand 1, whereas a slight tilting of ~4° is found in ligand 2.

The thermal stability of compounds **1–5** was investigated by DTA/TGA (Fig. 3 and Fig. S6–S9, ESI†). All compounds are stable up to approx. 100 °C with the exception of the Tm compound (**5**), which starts to decompose slightly below 100 °C (Fig. S9†). As an example the DTA/TGA of **3** shall be discussed in more detail (Fig. 3). A broad endothermic signal is observed between 150 °C and 200 °C. The mass loss of approx. 20% is in good agreement with the release of two DMF molecules (calculated mass loss: 21.6%). The third DMF molecule is obviously released during the strong exothermic event between 350 °C and 400 °C. The observed mass loss of approx. 35% points to a decomposition of the framework. The remaining mass at 450 °C (45% ≡ ~304 g mol^{-1}) is too high for simple residues like Tb_2O_3 ($M/2$ = 182.9 g mol^{-1}) or TbOF (M = 193.9 g mol^{-1}). Roughly similar results were obtained for compounds **1**, **2**, **4** and **5** (Fig. S6–S9, ESI†). Pronounced plateaus after DMF release are also observed for **4** and **5**. Thus, **3–5** are good candidates to follow the DMF release *via* temperature dependent XRPD, as for lower DMF contents a higher connectivity of the framework is expected. But also with respect to the luminescence properties of **3** (see below) a compound with a lower DMF content seems to be very interesting. Thus, these investigations are a part of our current research interests in this field. For **1** and **2** less pronounced DTA/TGA curves are found, so such investigations are less promising for these compounds.

Attempts to crystallize new coordination polymers under similar conditions as for **1–5** just by replacing DMF by formamide (FA) failed. But using a mechanochemical approach starting from the acetates and H_2tfBDC (see the Experimental section) led to the new compounds $^2_\infty[Ln^{III}(tfBDC)(CH_3COO)(FA)_3]\cdot 3FA$ with Ln^{III} = Sm^{3+} (**6**) and Eu^{3+} (**7**). Both are isostructural ($P\bar{1}$, Z = 2) so only compound **7** shall be discussed in detail. The asymmetric unit of **7** consists of one Eu^{3+} cation, one CH_3COO^- anion and six formamide molecules, all in general positions. Two crystallographically independent $tfBDC^{2-}$ anions are found. However, both are located on inversion centers, so that the full linkers are generated by this symmetry element. In Fig. 4 the coordination sphere around one Eu^{3+} cation is shown. Eu^{3+} is coordinated by nine oxygen atoms (CN = 9) stemming from three monodentately coordinating carboxylate groups of the $tfBDC^{2-}$ ligand (Eu–O: 235.6(2)–245.9(2) pm), one chelating bidentately coordinating (Eu–O: 252.7(2) pm and 259.4(2) pm) and one monodentately coordinating (Eu–O: 237.2(2) pm) carboxylate group of acetate

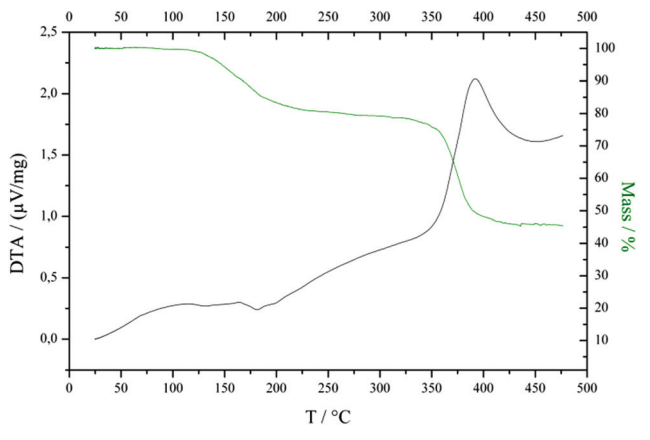

Fig. 3 DTA (black) and TGA (green) analysis of $^2_\infty[Tb^{III}(tfBDC)(NO_3)(DMF)_2]\cdot DMF$ (**3**).

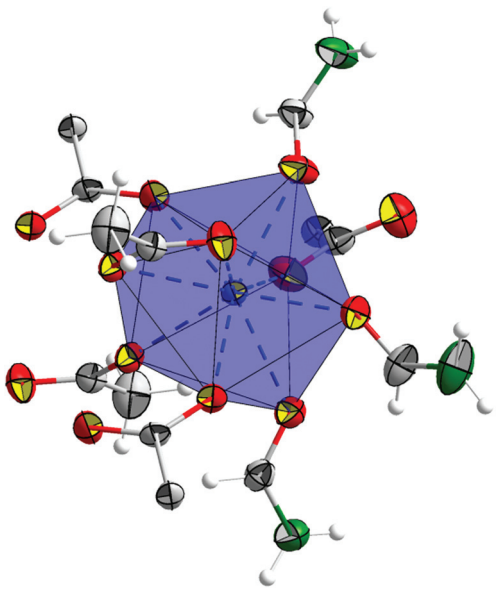

Fig. 4 ORTEP plot (50% probability) of the coordination sphere around Eu^{3+} in $^2_\infty[Eu^{III}(tfBDC)(CH_3COO)(FA)_3]\cdot 3FA$ (**7**); Eu (blue), O (red), C (light gray), N (green), H (small white spheres); the $tfBDC^{2-}$ ligand is only partly depicted.

anions, and three coordinating formamide (FA) molecules (Eu–O: 242.1(2) pm–250.4(2) pm). The next-nearest distance is Eu–C12 with 294.8(2) pm. The EuO_9 polyhedra are linked by a common edge and bridged by the carboxylate groups of two acetate anions to form dimeric units (Fig. 5). The Eu–Eu distance within these dimers is 405.85(3) pm (Eu–Eu in **1**: 406.67(8) pm). The Sm–Sm distances in **6** are, as expected, slightly larger: 408.05(7) pm. The same is found for the Sm–O distances (Table 3).

The dimeric $(EuO_{7/1}O_{2/2})_2$ units are connected *via* $tfBDC^{2-}$ ligands to form sheets, which are shown in Fig. 6. These layers are stacked along [010] in an AA fashion. The layers are held together by weak van der Waals forces. Non-coordinated formamide (FA) molecules (three per formula unit) fill the space in-between the layers so that no pores are found in this coordination polymer. Torsion angles between the benzene rings and the carboxylate groups of 69.3(1)° (2×) and 62.9(1)° (2×) are found for the two crystallographically independent $tfBDC^{2-}$ ligands. For symmetry reasons the carboxylate groups themselves are coplanar in both $tfBDC^{2-}$ ligands.

The DTA/TGA curves of **6** and **7** are given in the ESI (Fig. S13 and S14†). The release of formamide molecules starts slightly above 100 °C. For **7** a release of one formamide molecule should lead to a mass loss of 6.3%. So at approx. 200 °C the release of six formamide molecules seems to be finished. But as no clear plateau is reached, the solvent release seems to overlap with the decomposition of the framework. The remaining masses for **6** (approx. 30% at 500 °C) and **7** (approx. 43% at 300 °C) are higher than the expected values for 1/2 $Ln^{III}{}_2O_3$ (~24.5%) and $Ln^{III}OF$ (~26%). Thus, the mechanism of decomposition is unclear at the moment.

Single crystals of compounds $^2_\infty[Ln^{III}(tfBDC)(NO_3)(DMSO)_2]$ with Ln^{III} = Ho^{3+} (**8**), Er^{3+} (**9**) and Tm^{3+} (**10**) were obtained under similar conditions as compounds **1–5** by replacing DMF by DMSO. All compounds are isostructural (*Pbca*, $Z = 8$) so only compound **10** shall be discussed in the following. The asymmetric unit of **10** consists of one Tm^{3+} cation, one $tfBDC^{2-}$ anion, one NO_3^- anion and two DMSO molecules, all in general positions. In Fig. 7 the coordination sphere around one Tm^{3+} cation is shown. Tm^{3+} is coordinated by eight oxygen atoms (CN = 8) stemming from four monodentately coordinating carboxylate groups of the $tfBDC^{2-}$ ligand (Tm–O: 228.0(3)–234.9(3) pm), one chelating bidentately coordinating nitrate anion (Tm–O: 241.4(3) pm and 242.3(3) pm), and two coordinating DMSO molecules (Tm–O: 227.7(3) pm and 230.1(3) pm). The next-nearest distance is Tm–N3 with 283.7(5) pm. In contrast to compounds **1–7** these TmO_8 polyhedra are not linked directly, but bridged by chelating carboxylate groups of four $tfBDC^{2-}$ ligands (Fig. 8). Thus, a paddlewheel-like unit is formed. But as $tfBDC^{2-}$ anions are not coplanar for reasons mentioned above (torsion angles between the benzene ring and the carboxylate groups: 71.1(2)° and 77.2(2)°; torsion angle between both carboxylate groups: ~9°), the paddles of the paddlewheel are not parallel to its axis, but almost perpen-

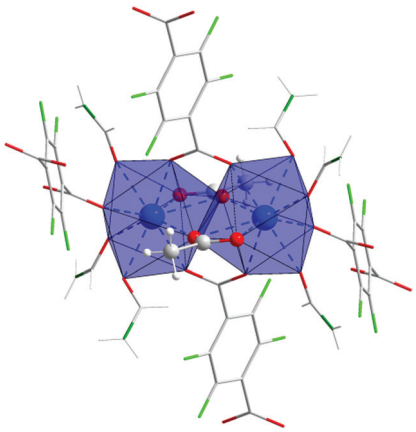

Fig. 5 Dimeric units in $^2_\infty[Eu^{III}(tfBDC)(CH_3COO)(FA)_3]\cdot 3FA$ (**7**); Eu^{3+} and CH_3COO^- are shown as balls and sticks, formamide (FA) and $tfBDC^{2-}$ as wires/sticks; Eu (blue), O (red), C (light gray), N (green), F (light green), H (white).

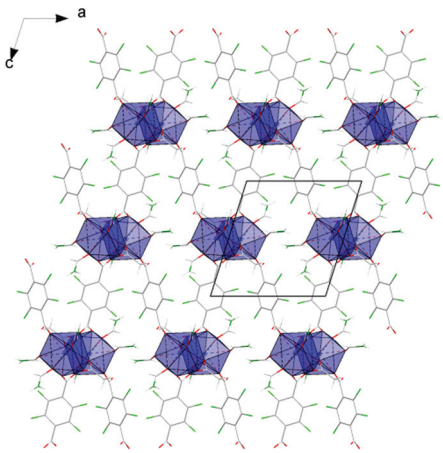

Fig. 6 View of a polymeric layer in the crystal structure of $^2_\infty[Eu^{III}(tfBDC)(CH_3COO)(FA)_3]\cdot 3FA$ (**7**) along [010]; all atoms and bonds are shown in a wire/stick representation; non-coordinating formamide (FA) molecules are omitted for clarity; color coding as in Fig. 5.

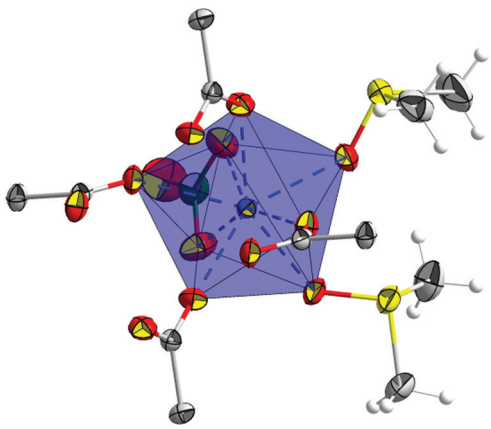

Fig. 7 ORTEP plot (50% probability) of the coordination sphere around Tm^{3+} in $^2_\infty[Tm^{III}(tfBDC)(NO_3)(DMSO)_2]$ (**10**); Tm (blue), O (red), C (light gray), N (green), S (yellow), H (small white spheres); the $tfBDC^{2-}$ ligand is only partly depicted.

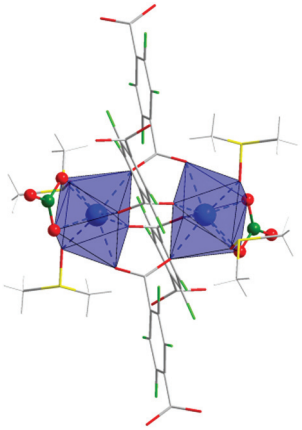

Fig. 8 Dimeric units in $^{2}_{\infty}[Tm^{III}(tfBDC)(NO_3)(DMSO)_2]$ (**10**); Tm^{3+} and NO_3^- are shown as balls and sticks, DMSO and $tfBDC^{2-}$ as wires/sticks; Tm (blue), O (red), C (light gray), N (green), F (light green), S (yellow), H (white).

dicular to it. The Tm–Tm distance within these dimers is significantly enhanced compared to **1–7** (Table 3): Tm–Tm = 439.48(5) pm in **10** compared to Eu–Eu = 405.85(3) pm in **7** and 406.67(8) pm in **1**. The Ln^{III}–Ln^{III} distances as well as the Ln^{III}–O distances in **8** and **9** are, as expected, slightly larger than in **10** (Table 3). It is noteworthy that the spread of the Ln^{III}–O distances in **8–10** is significantly smaller than in compounds **1–7** (Table 3). This points to a higher symmetric coordination sphere around Ln^{3+} in **8–10** and might be attributed to the fact that no non-coordinating solvent molecules are found in these compounds.

The dimeric $(TmO_8)_2$ units in **10** are connected *via* $tfBDC^{2-}$ ligands to form sheets in the (001) plane, which are shown in Fig. 9. These 4^4 nets are stacked along [001] in an AB fashion with a translation vector $\sim\frac{1}{2}\,\frac{1}{2}\,\frac{1}{2}$, so that the dimers of the next layer are positioned above the center of the square grids of the

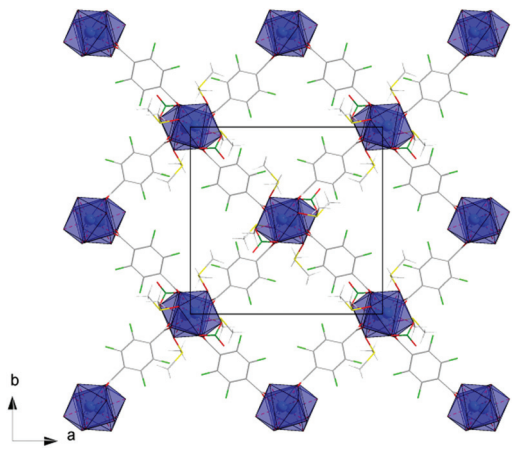

Fig. 9 View of a polymeric layer in the crystal structure of $^{2}_{\infty}[Tm^{III}(tfBDC)(NO_3)(DMSO)_2]$ (**10**) along [001]; all atoms with the exception of Tm and bonds are shown in a wire/stick representation; color coding as in Fig. 8.

layer below. The layers are held together by weak van der Waals forces. In Fig. S24 (ESI†) a space-filling presentation of these layers is given. No non-coordinating solvent molecules are found to fill the empty space shown in Fig. S24† (*cp.* low residual electron density given in Table 2). Thus, compounds **8–10** might be candidates showing permanent porosity and gas sorption properties. Such properties have already been found for similar systems composed of polymeric layers.[25] Such investigations on compounds **8–10** will be performed in the near future.

The DTA/TGA curves of compounds **9** and **10** are given in the ESI (Fig. S19 and S20†). **9** and **10** are more stable than **1–7**. The release of solvent molecules starts above 150 °C. This is due to the fact that the crystal structures of **9** and **10** do not contain non-coordinating solvent molecules like **1–7**. For **10** (**9** shows similar results) an endothermic event is found around 200 °C with a mass loss of approx. 12.8%. For the loss of one DMSO molecule a mass loss of 12.5% is calculated. An almost flat plateau after the release of one DMSO molecule makes **10** an interesting candidate to follow DMSO release *via* temperature dependent XRPD, as for lower DMSO contents a higher connectivity of the framework can be expected. A second, strong exothermic event is observed at approx. 370 °C. The high mass loss points to a release of the second DMSO molecule accompanied by a decomposition of the compound. The remaining mass at 450 °C (47% ≡ ~293 g mol^{-1}) is too high for simple residues like Tm_2O_3 ($M/2$ = 192.9 g mol^{-1}) or TmOF (M = 203.9 g mol^{-1}). To analyze this residue **9** was heated to 500 °C under an argon atmosphere. Elemental (CHNS) analysis of the resulting black powder gave approx. 17 weight% carbon, but no nitrogen, sulfur or hydrogen. The XRPD (ESI: Fig. S30†) of this residue showed several broad reflections, which can be assigned to ErF_3. Only one very broad reflection at $2\theta \approx 4.7°$ seems to belong to rhombohedral graphite, which explains the carbon found in the elemental analysis.

To sum up the crystal structure analyses all known crystal structures of coordination polymers containing Ln^{3+} cations and $tfBDC^{2-}$ linkers have been compared.[7,11,12,26–28] They are summarized in Table 4. Surprisingly, only in our work (ref. 11, this work), it was found that additional anions like NO_3^- or CH_3COO^- are incorporated in the crystal structures of coordination polymers. Larionov *et al.* started from freshly prepared $Ln(OH)_3$,[26,27] but in the work of Mikhalyova *et al.*,[28] MacNeill *et al.*,[12] and Chen *et al.*[7] synthetic procedures similar to ours were used. So the choice of solvents – addition of water,[7] MeOH instead of EtOH,[28] or DEF instead of DMF[12] – and the reaction temperature −80 °C in ref. 7, all others at RT – seem to influence the incorporation of NO_3^- anions, as the solubility of nitrates is changed. Our new mechanochemical synthesis starting from $Ln(CH_3COO)_3{\cdot}H_2O$ and H_2tfBDC seems to be an interesting approach to incorporate acetate anions (this work). The coordination numbers of Ln^{3+} cations mainly follow the size of the cations: for the larger lanthanides CN = 9 is preferred, whereas for smaller lanthanides CN = 8 is also found. Only the structure type $^{2}_{\infty}[Ln^{III}(tfBDC)(NO_3)(DMF)_2]{\cdot}DMF$ (type IV, Table 4) seems to be very flexible, as here CN = 9 is found

for almost all lanthanides (ref. 11, this work). A common feature of all compounds are binuclear units, which seem to be the preferred structural unit in the crystal chemistry of coordination polymers with Ln^{3+} and $tfBDC^{2-}$ linkers. In all types (Table 4) with the exception of type I these binuclear units are connected by $tfBDC^{2-}$ ligands in two directions to form a layer-like polymer. Despite these similarities, in detail the dimers differ significantly with respect to the coordination number, surrounding of Ln^{3+} cations and connection of the monomers to dimers (connection *via* edges in types III, IV, VI and *via* faces in types II, VII; the different connectivity of type V is shown in Fig. 8). Most strikingly, the stacking of the layers is different, as shown for compounds **1–10** in this manuscript. But still, at the moment the crystal chemistry of coordination polymers with Ln^{3+} and $tfBDC^{2-}$ linkers is less multifaceted than that of coordination polymers of Ln^{3+} and non-fluorinated BDC^{2-} linkers, as described by Mikhalyova *et al.*[28] The only 3D polymer up to now is $^3_\infty[Er(tfBDC)_{3/2}(DMF)_{1/2}(H_2O)_{1/2}]\cdot\frac{1}{2}DMF$ (type I).[7] Here, $(Er1)_2$ (Er1–Er1: 378.35(5) pm) and $(Er2)_2$ dimers (Er2–Er2: 379.91(5) pm) connected *via* common edges are further connected to rod-like chains by two bridging carboxylate groups of $tfBDC^{2-}$ ligands (Er1–Er2: 500.33(7) pm). These rods are interconnected by $tfBDC^{2-}$ ligands in two directions to form a 3D framework structure.

It was already shown that coordination polymers with perfluorinated linkers give rise to strong emission, as quenching due to C–H-related vibronic states is reduced.[7,11] Previous work, however, was restricted to Pr^{3+}, Sm^{3+}, Dy^{3+}, and Er^{3+} containing compounds. The bright red and green photoluminescence of Eu^{3+} and Tb^{3+} containing coordination polymers has also been investigated.[12,26,27] But to the best of our knowledge, a quantitative analysis of the quantum yield has never been performed up to now. Irradiating compounds **1** and **3** with UV light resulted in a bright red (**1**) and green (**3**) luminescence, as shown in the insets of Fig. 10 and 11. Excitation spectra of **1** (ESI: Fig. S25†) show that the maximum emission band with Λ_{max} = 618 nm was excited. The spectrum shows a typical $^5D_0 \rightarrow {}^7F_2$ transition, also known as hypersensitive electric dipole transition that is characteristic

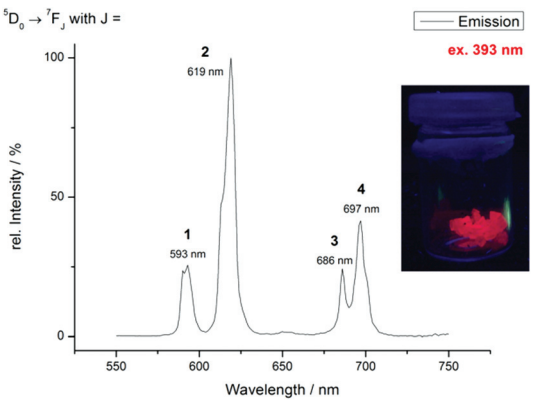

Fig. 10 Emission spectrum of **1** (Λ_{ex} = 393 nm); inset: intense red emission of single crystals of **1**.

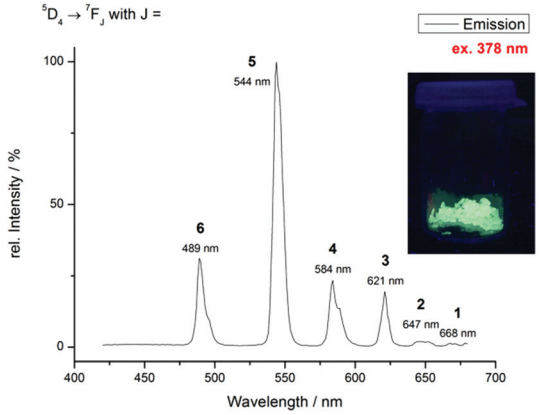

Fig. 11 Emission spectrum of **3** (Λ_{ex} = 378 nm); inset: intense green emission of single crystals of **3**.

for Eu^{3+} ions located on centers of symmetry, as found in the crystal structure of **1**. Further excitation bands were observed for $^5D_1$, $^5D_0$, $^5L_6$, $^5G_2$, $^5L_7$, $^5G_{3,4,5,6}$ and $^5D_4$ transitions. A broad band around 298 nm indicates the absorption of the $tfBDC^{2-}$ linker.

The emission spectrum of **1** (Fig. 10; Λ_{ex} = 393 nm) reveals several f–f-transitions $^5D_0 \rightarrow {}^7F_J$ with J = 1, 2, 3, 4. The most intensive band arises from the hypersensitive transition $^5D_0 \rightarrow {}^7F_2$ (619 nm), which is, as mentioned, very sensitive to its chemical environment and responsible for the bright red color of the luminescence. Further weaker emission bands were observed at Λ_{em} = 686/697 nm ($^5D_0 \rightarrow {}^7F_4$), at 650 nm ($^5D_0 \rightarrow {}^7F_3$) and at 590/593 nm ($^5D_0 \rightarrow {}^7F_1$). $^5D_0 \rightarrow {}^7F_1$ and $^5D_0 \rightarrow {}^7F_3$ transitions are magnetic dipole transitions that are independent of their chemical environment, so it is possible to use their intensities as a standard to compare the intensities of other transitions.

The relative quantum yields were determined with an integrating sphere ("Ulbricht sphere"). During a day a decrease of the quantum yield from 45% to 9% was observed. After one hour at 60 °C, a maximum quantum yield of 53% was obtained. The DTA/TG curve of **1** reveals that the sample is stable up to 100 °C and higher. So we assume that **1** takes up water from the atmosphere, which quenches the luminescence *via* O–H vibrations. Attempts to excite **1** *via* the $tfBDC^{2-}$ linker have not been successful up to now. But this is part of our ongoing work in this field with a special focus on energy transfer *via* the linker to the next Ln^{3+} center.

Excitation and emission spectra of **3** (ESI: Fig. S26,† Fig. 11) show typical Tb^{3+} transitions. If excited at 378 nm, the following transitions occur: $^5D_4 \leftarrow {}^7F_6$, $^5D_3 \leftarrow {}^7F_6$, $^5G_6 \leftarrow {}^7F_6$, $^5L_{10} \leftarrow {}^7F_6$, $^5G_5 \leftarrow {}^7F_6$, $^5L_9 \leftarrow {}^7F_6$, $^5G_4 \leftarrow {}^7F_6$, $^5D_1 \leftarrow {}^7F_6$ and $^5D_2 \leftarrow {}^7F_6$. The absorption band of the $tfBDC^{2-}$ linker overlaps with the strong and broad $^5D_1 \leftarrow {}^7F_6$ transition. Only a weak shoulder at 298 nm is observed. The emission spectrum of **3** (Λ_{ex} = 378 nm) is dominated by a strong band at 544 nm that is responsible for the bright green emission. The following transitions are observed: $^5D_4 \rightarrow {}^7F_J$ with J = 1, 2, 3, 4, 5, 6. The first

two are very weak, whereas the transition with $J = 5$ gives rise to the strong band at 544 nm.

The maximum quantum yield obtained for **3** was 67%. Similar to **1** the quantum yield decreased if exposed to air for longer times. A sample having a minimum quantum yield of 35% was heated at 60 °C for one hour, which increased its quantum yield to 49%. Like for **1**, we assume that moisture from the atmosphere decreases the quantum yield by O-H quenching significantly. These results were obtained for samples containing larger crystals. But measurements on powdered samples gave similar results with a lower quantum yield, in general. Again, attempts to excite **3** *via* the $tfBDC^{2-}$ linker have not been successful up to now.

To investigate the influence of solvent molecules on the luminescence properties, excitation (Fig. S27, ESI†) and emission spectra (Fig. 12) of **7** were recorded. Like compound **1**, **7** contains Eu^{3+} cations and $tfBDC^{2-}$ linkers, but NO_3^- is replaced by CH_3COO^-, and DMF by formamide. Based on the simple picture of C–H-related quenching, one expects a weaker luminescence of **7**, as CH_3COO^- coordinates directly to Eu^{3+}. This expectation is fulfilled, as a quantum yield as low as 10% was observed for **7**. The excitation spectrum of **7**, measured at $\Lambda_{em,max}$ = 618 nm, shows the following transitions: $^5D_1$, $^5D_0$, $^5L_6$, $^5G_2$, $^5L_7$, $^5L_6$, $^5G_{3,4,5,6}$, $^5D_4$ as well as a broader band at 317 nm that could not be assigned to any reasonable transition. The absorption band of the $tfBDC^{2-}$ linker seems to start below 300 nm and is thus significantly shifted as compared to **1**. The emission spectrum of **7** (Fig. 12), excited at 393 nm, shows $^5D_0 \rightarrow {}^7F_J$ transitions with J = 1–4. The most intensive band at Λ_{max} = 592 nm ($J = 1$) is surprisingly stronger than the band at 618 nm ($J = 2$). The latter is a hypersensitive transition, typical for Eu^{3+}.

Fig. S28 and S29 (ESI†) show comparisons of the excitation and emission spectra of **1** and **7**, setting the strongest band of each spectrum to 100%. Different intensities indicate different coordination spheres and symmetries in both compounds. In the excitation spectra a broad band for the $tfBDC^{2-}$ linker at 298 nm for **1** seems to be shifted to higher energies for **7**. Furthermore, the intensity of the $^5D_0 \rightarrow {}^7F_2$ transition in **1** (emission spectrum) is significantly higher than in **7**, which is also reflected in the higher quantum yield of **1** compared to **7**.

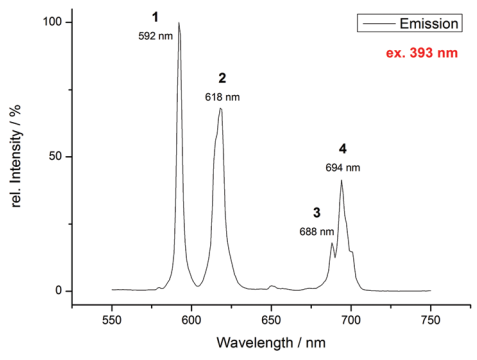

Fig. 12 Emission spectrum of **7**.

Experimental

General remarks

Tetrafluoroterephthalic acid (H_2tfBDC) was prepared according to the procedure described in the literature.[9]

$Er(NO_3)_3{\cdot}5H_2O$, $Eu(CH_3COO)_3{\cdot}H_2O$, $Eu(NO_3)_3{\cdot}6H_2O$, $Gd(NO_3)_3{\cdot}6H_2O$, $Ho(NO_3)_3{\cdot}5H_2O$, $Sm(CH_3COO)_3{\cdot}H_2O$, $Tb(NO_3)_3{\cdot}6H_2O$, $Tm(NO_3)_3{\cdot}6H_2O$ (all from ABCR), *N*,*N*′-dimethylformamide (KMF LaborchemieHandels GmbH), formamide (Alfa Aesar), dimethyl sulfoxide (VWR BDH Prolabo), ethanol (Biesterfeld) and triethylamine (Acros Organics) were used as purchased, without any further purification. In all syntheses, yields were not optimized and, therefore, are not given.

Syntheses

Compounds with the composition $^2_\infty[Ln^{III}(tfBDC)(NO_3)(DMF)_2]{\cdot}DMF$ with $Ln^{III} = Eu^{3+}$ (**1**), Gd^{3+} (**2**), Tb^{3+} (**3**), Ho^{3+} (**4**) and Tm^{3+} (**5**) were synthesized as follows:

1.5 mmol (1.4 equiv.) $Ln^{III}(NO_3)_3{\cdot}xH_2O$ and 1.1 mmol (1.0 equiv.) H_2tfBDC were dissolved in 10 mL of a solvent mixture of ethanol and *N*,*N*′-dimethylformamide (3 : 1, v : v). The snap-cap tube was closed with a cap and the latter was perforated once. It was placed in an exsiccator, whose bottom was filled with 100 mL of the solvent mixture mentioned above. In addition, a beaker with 20 mL of triethylamine dissolved in 20 mL of the same solvent mixture was placed in the exsiccator. After one month, colorless crystals of **1**, **2**, **3** and **5** and pink crystals of **4** several millimeters in size were obtained.

Elemental analysis for **1**: Found: C, 29.7; H, 3.5; N, 8.6. Calc. for $EuC_{17}H_{21}O_{10}F_4N_4$: C, 30.5; H, 3.2; N, 8.4%. Purity was additionally checked by XRPD (Fig. S1 in the ESI†). Both investigations indicate that a single-phase sample was obtained.

Elemental analysis for **2**: Found: C, 29.9; H, 3.6; N, 8.6. Calc. for $GdC_{17}H_{21}O_{10}F_4N_4$: C, 30.3; H, 3.1; N, 8.3%. Purity was additionally checked by XRPD (Fig. S2 in the ESI†). Weak additional reflections indicate a small amount of an unknown impurity. Therefore, only the results of the X-ray single-crystal structure analysis of **2** are discussed.

Elemental analysis for **3**: Found: C, 30.4; H, 3.6; N, 8.1. Calc. for $TbC_{17}H_{21}O_{10}F_4N_4$: C, 30.2; H, 3.1; N, 8.2%. Purity was additionally checked by XRPD (Fig. S3 in the ESI†). Both investigations indicate that a single-phase sample was obtained.

Elemental analysis for **4**: Found: C, 28.7; H, 3.3; N, 7.4. Calc. for $HoC_{17}H_{21}O_{10}F_4N_4$: C, 29.9; H, 3.1; N, 8.2%. Purity was additionally checked by XRPD (Fig. S4 in the ESI†). The latter does not show any impurity reflections, but due to the modest elemental analysis only the results of the X-ray single-crystal structure analysis of **4** are discussed.

Elemental analysis for **5**: Found: C, 28.2; H, 3.1; N, 6.8. Calc. for $TmC_{17}H_{21}O_{10}F_4N_4$: C, 29.8; H, 3.1; N, 8.2%. Purity was additionally checked by XRPD (Fig. S5 in the ESI†). Both investigations indicate that no single-phase sample was obtained. Therefore, only the results of the X-ray single-crystal structure analysis of **5** are discussed.

IR data (KBr pellets) of **1**–**5** are presented in Fig. S10 and Table S1 in the ESI.†

Compounds with the composition $^{2}_{\infty}[Ln^{III}(tfBDC)(CH_3COO)(FA)_3]\cdot 3FA$ with $Ln^{III} = Sm^{3+}$ (**6**) and Eu^{3+} (**7**) were synthesized applying a mechanochemical approach: 3 mmol (2.0 equiv.) $Ln^{III}(CH_3COO)_3\cdot H_2O$ were ground with 1.5 mmol (1.0 equiv.) H_2tfBDC, until no smell of acetic acid was noticed any longer. The residue was dissolved in 60 ml formamide (FA). After approx. one week single crystals of **6** and **7** were obtained after slow evaporation of the solvent.

Elemental analysis for **6**: Found: C, 26.4; H, 2.7; N, 11.9. Calc. for $SmC_{16}H_{21}F_4N_6O_{12}$: C, 26.9; H, 3.0; N, 11.7%. Purity was additionally checked by XRPD (Fig. S11 in the ESI†). Both investigations indicate that a single-phase sample was obtained.

Elemental analysis for **7**: Found: C, 26.4; H, 3.0; N, 11.1. Calc. for $EuC_{16}H_{21}F_4N_6O_{12}$: C, 26.8; H, 3.0; N, 11.7%. Purity was additionally checked by XRPD (Fig. S12 in the ESI†). Both investigations indicate that a single-phase sample was obtained.

IR data (KBr pellets) of **6** and **7** are presented in Fig. S15 and Table S2 in the ESI.†

Compounds with the composition $^{2}_{\infty}[Ln^{III}(tfBDC)(NO_3)(DMSO)_2]$ with $Ln^{III} = Ho^{3+}$ (**8**), Er^{3+} (**9**) and Tm^{3+} (**10**) were synthesized by a similar synthesis described for compounds **1–5**. 1.5 mmol (1.4 equiv.) $Ln^{III}(NO_3)_3\cdot xH_2O$ and 1.1 mmol (1.0 equiv.) H_2tfBDC were dissolved in 10 mL of a solvent mixture of ethanol and dimethyl sulfoxide (3 : 1, v : v). The snap-cap tube was closed with a cap and the latter was perforated once. It was placed in an exsiccator, whose bottom was filled with 100 mL of the solvent mixture mentioned above. In addition, a beaker with 20 mL of triethylamine dissolved in 20 mL of the same solvent mixture was placed in the exsiccator. After 1–2 months pink crystals of **8** and **9** and colourless crystals of **10** were obtained.

Elemental analysis for **8**: Found: C, 23.1; H, 2.5; N, 2.5; S, 10.1. Calc. for $HoC_{12}F_4S_2O_9N$: C, 23.3; H, 2.0; N, 2.6; S, 10.4%. Purity was additionally checked by XRPD (Fig. S16 in the ESI†). Both investigations indicate that a single-phase sample was obtained.

Elemental analysis for **9**: Found: C, 22.2; H, 2.5; N, 2.2; S, 7.9. Calc. for $ErC_{12}F_4S_2O_9N$: C, 23.2; H, 2.0; N, 2.3; S, 10.3%. Purity was additionally checked by XRPD (Fig. S17 in the ESI†). Both investigations indicate that no single-phase sample was obtained.

Elemental analysis for **10**: Found: C, 22.3; H, 2.3; N, 2.3; S, 7.1. Calc. for $TmC_{12}F_4S_2O_9N$: C, 23.1; H, 1.9; N, 2.3; S, 10.3%. Purity was additionally checked by XRPD (Fig. S18 in the ESI†). The elemental analysis indicates that no single-phase sample was obtained.

IR data (KBr pellets) of **8–10** are presented in Fig. S21 and Table S3 in the ESI.†

X-Ray single crystal structure analysis

Single crystals of **1–10** were isolated and mounted in sealed glass capillaries on a Stoe IPDS I or IPDS II diffractometer ($T \approx 293$ K, Mo Kα radiation). For data collection and reduction the Stoe program package[13] was used. The structural models were solved using SIR-92[14] and completed using difference Fourier maps calculated with SHELXL-97,[15] which was also used for final refinements. These programs were run under the WinGX system.[16] All non-hydrogen atoms were refined anisotropically. Hydrogen atoms of solvent molecules and acetate groups were placed in calculated positions and refined "riding" with fixed distances (93 pm (C(O)H group), 96 pm (CH_3 group), 86 pm (NH_2 group)). Details of all single-crystal structure analyses are given in Tables 1 and 2.[17]

Table 1 Details of X-ray single crystal structure analysis of compounds **1–5**

Formula	$EuC_{17}H_{21}F_4N_4O_{10}$	$GdC_{17}H_{21}F_4N_4O_{10}$	$TbC_{17}H_{21}F_4N_4O_{10}$	$HoC_{17}H_{21}F_4N_4O_{10}$	$TmC_{17}H_{21}F_4N_4O_{10}$
Formula weight [g mol^{-1}]	669.34	674.63	676.30	682.31	686.31
Crystal description	Block, colorless	Block, colorless	Block, colorless	Block, pink	Block, colorless
Crystal size [mm]	0.50 × 0.20 × 0.20	0.60 × 0.50 × 0.30	0.40 × 0.25 × 0.15	0.30 × 0.25 × 0.20	0.70 × 0.50 × 0.30
Space group, Z	$C2/c$ (no. 15), 8	$C2/c$ (no. 15), 8	$C2/c$ (no. 15), 8	$C2/c$ (no. 15), 8	$C2/c$ (no. 15), 8
a [pm]	2208.5(3)	2211.8(4)	2215.7(3)	2204.7(4)	2200.7(2)
b [pm]	1139.40(13)	1139.96(16)	1136.80(13)	1132.19(15)	1127.42(10)
c [pm]	2057.8(3)	2057.0(4)	2056.6(3)	2051.5(6)	2048.4(2)
β [°]	111.243(11)	111.147(17)	111.047(11)	111.38(2)	111.459(8)
V [×10^6 pm^3]	4826.3(11)	4837.2(15)	4834.6(11)	4768.4(18)	4730.0(8)
Calc. density [g cm^{-3}]	1.842	1.853	1.858	1.901	1.928
Absorption correction	Numerical	Numerical	Numerical	Numerical	Numerical
Diffractometer (all Mo Kα radiation)	Stoe IPDS I	Stoe IPDS I	Stoe IPDS II	Stoe IPDS I	Stoe IPDS I
Temperature [K]	293(2)	293(2)	293(2)	293(2)	293(2)
$2\theta_{max}$ [°]	56.2	56.2	54.6	56.4	54.4
Index ranges	$-29 \le h \le 28$ $-14 \le k \le 14$ $-27 \le l \le 15$	$-29 \le h \le 28$ $-14 \le k \le 15$ $-27 \le l \le 25$	$-28 \le h \le 28$ $-14 \le k \le 14$ $-26 \le l \le 26$	$-28 \le h \le 29$ $-14 \le k \le 14$ $-27 \le l \le 27$	$-28 \le h \le 28$ $-14 \le k \le 14$ $-23 \le l \le 26$
Reflections: measured/independent	9149/5224	10 905/4124	11 978/3977	10 838/4073	17 808/3914
Significant reflections	3597 with $I > 2\sigma(I)$	2085 with $I > 2\sigma(I)$	2827 with $I > 2\sigma(I)$	2616 with $I > 2\sigma(I)$	3493 with $I > 2\sigma(I)$
R(int)	0.032	0.152	0.088	0.102	0.089
Parameters/restraints	335/0	335/0	337/0	335/0	336/0
GooF = S_{all}	0.92	0.81	0.89	0.92	1.04
$R[F^2 > 2\sigma(F^2)]$	0.033	0.064	0.044	0.070	0.029
w$R(F^2)$	0.075	0.144	0.116	0.180	0.079
$\Delta\rho_{max}/\Delta\rho_{min}$ [e × 10^{-6} pm^{-3}]	−1.38/1.08	−1.77/2.37	−0.83/0.85	−3.22/3.95	−1.41/1.40

Table 2 Details of X-ray single crystal structure analysis of compounds **6–10**

Formula	$SmC_{16}H_{21}F_4N_6O_{12}$	$EuC_{16}H_{21}F_4N_6O_{12}$	$HoC_{12}H_{12}F_4NO_9S_2$	$ErC_{12}H_{12}F_4NO_9S_2$	$TmC_{12}H_{12}F_4NO_9S_2$
Formula weight [g mol^{-1}]	715.74	717.35	619.28	621.61	623.28
Crystal description	Block, yellow	Block, colorless	Block, pink	Block, pink	Block, colorless
Crystal size [mm]	0.30 × 0.30 × 0.20	0.30 × 0.20 × 0.20	0.20 × 0.10 × 0.10	0.45 × 0.30 × 0.25	0.40 × 0.20 × 0.10
Space group, Z	$P\bar{1}$, 2	$P\bar{1}$, 2	*Pbca*, 8	*Pbca*, 8	*Pbca*, 8
a [pm]	1098.16(13)	1094.65(5)	1546.09(17)	1541.77(13)	1535.08(4)
b [pm]	1116.45(13)	1111.55(5)	1505.99(15)	1504.82(9)	1496.76(4)
c [pm]	1152.91(12)	1146.84(5)	1670.57(15)	1667.49(11)	1657.58(6)
α [°]	101.818(9)	101.707(3)	90	90	90
β [°]	104.289(9)	104.300(3)	90	90	90
γ [°]	101.705(9)	101.651(3)	90	90	90
V [×10^6 pm^3]	1292.0(3)	1276.49(10)	3889.7(7)	3868.7(5)	3808.5(2)
Calc. density [g cm^{-3}]	1.840	1.866	2.115	2.134	2.174
Absorption correction	Numerical	Numerical	Numerical	Numerical	Numerical
Diffractometer (all Mo Kα radiation)	Stoe IPDS II	Stoe IPDS II	Stoe IPDS II	Stoe IPDS II	Stoe IPDS II
Temperature [K]	293(2)	293(2)	293(2)	293(2)	293(2)
$2\theta_{max}$ [°]	59.0	58.4	54.6	54.6	53.6
Index ranges	$-15 \le h \le 15$ $-15 \le k \le 15$ $-15 \le l \le 15$	$-12 \le h \le 15$ $-15 \le k \le 15$ $-15 \le l \le 15$	$-19 \le h \le 19$ $-19 \le k \le 19$ $-21 \le l \le 21$	$-19 \le h \le 19$ $-19 \le k \le 18$ $-18 \le l \le 21$	$-19 \le h \le 19$ $-18 \le k \le 18$ $-20 \le l \le 20$
Reflections: measured/independent	25 552/7176	20 469/6852	50 858/4107	40 534/4305	43 741/3828
Significant reflections	5383 with $I > 2\sigma(I)$	6422 with $I > 2\sigma(I)$	2159 with $I > 2\sigma(I)$	3635 with $I > 2\sigma(I)$	2952 with $I > 2\sigma(I)$
R(int)	0.088	0.037	0.188	0.045	0.097
Parameters/restraints	353/0	353/0	266/0	267/0	266/0
GooF = S_{all}	1.08	1.07	0.90	1.11	1.03
$R[F^2 > 2\sigma(F^2)]$	0.046	0.023	0.047	0.035	0.028
w$R(F^2)$	0.086	0.060	0.075	0.101	0.069
$\Delta\rho_{max}/\Delta\rho_{min}$ [e × 10^{-6} pm^{-3}]	−2.06/1.02	−0.86/0.74	−1.25/1.03	−1.67/1.17	−1.59/0.70

Table 3 Ionic radii and selected interatomic distances of compounds **1–10**

Ln^{3+} ion	Corresponding compound	Ionic radii[19] [pm]	Interatomic distances [pm]		
			Ln^{3+}–Ln^{3+}	Ln^{3+}–O	$\Delta[(Ln^{III}–O)_{max}–(Ln^{III}–O)_{min}]$
Eu^{3+}	**1**	126.0 (CN = 9)	406.67(8)	238.7(4)–262.3(3)	23.6
Gd^{3+}	**2**	124.7 (CN = 9)	404.6(2)	238.1(11)–262.0(7)	23.9
Tb^{3+}	**3**	123.5(CN = 9)	402.84(8)	235.1(6)–260.4(5)	25.3
Ho^{3+}	**4**	121.2 (CN = 9)	402.0(1)	233.1(8)–261.9(9)	28.8
Tm^{3+}	**5**	119.2 (CN = 9)	399.98(5)	231.0(3)–261.0(3)	30.0
Sm^{3+}	**6**	127.2 (CN = 9)	408.05(7)	236.8(3)–260.1(3)	23.3
Eu^{3+}	**7**	126.0 (CN = 9)	405.85(3)	235.5(2)–259.4(2)	23.9
Ho^{3+}	**8**	115.5 (CN = 8)	443.33(6)	229.4(6)–244.2(7)	14.8
Er^{3+}	**9**	114.4 (CN = 8)	441.08(5)	229.0(4)–243.6(4)	14.6
Tm^{3+}	**10**	113.4 (CN = 8)	439.48(5)	227.7(3)–242.2(4)	14.5

Table 4 Known crystal structures of coordination polymers containing Ln^{3+} cations and $tfBDC^{2-}$ linkers

Type	General composition	Reference: Ln^{3+}	Space group, Z	Coordination number (CN)
I	$^3_\infty[Ln^{III}(tfBDC)_{3/2}(DMF)_{1/2}(H_2O)_{1/2}]\cdot\frac{1}{2}DMF$	Ref. 7: Er^{3+}	$P\bar{1}$, 4	8
II	$^2_\infty[Ln^{III}(tfBDC)_{3/2}(DMF)]\cdot H_2O$	Ref. 27: Pr^{3+}, Nd^{3+}	$C2$, 4	9
III	$^2_\infty[Ln^{III}(tfBDC)_{3/2}(DEF)(EtOH)]\cdot DEF$	Ref. 12: La^{3+}, Nd^{3+}, Eu^{3+}, Gd^{3+}, Tb^{3+}	$C2/c$, 8	9
IV	$^2_\infty[Ln^{III}(tfBDC)(NO_3)(DMF)_2]\cdot DMF$	Ref. 11: Ce^{3+}, Pr^{3+}, Nd^{3+}, Sm^{3+}, Dy^{3+}, Er^{3+}, Yb^{3+} This work: Eu^{3+}, Gd^{3+}, Tb^{3+}, Ho^{3+}, Tm^{3+}	$C2/c$, 8	9
V	$^2_\infty[Ln^{III}(tfBDC)(NO_3)(DMSO)_2]$	This work: Ho^{3+}, Er^{3+}, Tm^{3+}	*Pbca*, 8	8
VI	$^2_\infty[Ln^{III}(tfBDC)(CH_3COO)(FA)_3]\cdot 3FA$	This work: Sm^{3+}, Eu^{3+}	$P\bar{1}$, 2	9
VII	$^2_\infty[Ln^{III}(tfBDC)_{3/2}(H_2O)_2]\cdot H_2O$	Ref. 25: Tb^{3+} Ref. 26: Sm^{3+}, Eu^{3+}, Dy^{3+}	$C2$, 4	9

X-Ray powder diffraction

XRPD data were collected at room temperature on a Huber G670 diffractometer (germanium monochromator, CuKα_1 radiation, imaging plate detector). To minimize the strong absorption of all compounds, measurements were carried out as flat samples with the substances placed between two foils (reflec-

tions due to the foil: $2\theta \approx 21.5°$ and $2\theta \approx 23.7°$). Typical recording times range from 60 min (compounds **6** and **7**) to 720 min (compounds **1–5** and **8–10**). Employing the WinXPow software suite,[18] the recorded patterns were compared with theoretical patterns calculated from single-crystal structure data.

Elemental analysis

Elemental analyses were carried out with HEKAtech CHNS Euro EA 3000.

Thermoanalytical investigations

Differential thermal analyses (DTA) and thermogravimetric analyses (TGA) were performed in Al_2O_3 containers (typical sample masses: approx. 20 mg). The temperature intervals were 25–300 °C and 25–500 °C, resp. with heating rates of 10–20 °C min^{-1}. The instrument (Netzsch STA 409C) is housed in a glovebox (M. Braun, Garching/Germany, nitrogen atmosphere) and the sample chamber is continuously flushed with argon at a rate of 70 ml min^{-1}.

Infrared spectroscopy

IR measurements were carried out on KBr pellets using Bruker IFS 66v/S with a Nernst globar.

Absorption

Visible and NIR absorption spectra were measured at room temperature on a Cary 5000 spectrometer (Varian, Palo Alto, USA). For the measurements, pellets of solid samples were prepared and fixed in the sample holder.

Luminescence spectroscopy

Excitation and emission spectra were recorded using a HORIBA Jobin Yvon Fluorolog 3 photoluminescence spectrometer equipped with a continuous 450 W xenon lamp, double monochromators for excitation and emission beams, an integrating sphere (Ulbricht sphere), and a photomultiplier tube (PMT) as the detector. Excitation and emission spectra were corrected using standard corrections, including the spectral intensity distribution of the lamp, the reflection behavior of the Ulbricht sphere, and the sensitivity of the detector. Determination of the absolute quantum yield was performed as suggested by Friend and co-workers.[20–22] All samples were investigated as solids in spectroscopically pure quartz cuvettes in the front-face mode. For the measurements, crystals were freshly taken from the supernatant solvent mixture, dried with tissue, ground and filled in the cuvettes.

Conclusion

To conclude, we have been able to synthesize and characterize ten new coordination polymers based on lanthanide cations and tetrafluoroterephthalate ($tfBDC^{2-}$) linkers. Three different structure types were obtained depending on the solvent (DMF, DMSO, formamide) and the anion (NO_3^-, CH_3COO^-). In all compounds binuclear units connected to polymeric layers were found, which however showed several differences: *e.g.* different coordination numbers and different stacking of the layers. Bright luminescence is found in $^2_\infty[Ln^{III}(tfBDC)(NO_3)(DMF)_2]\cdot DMF$ with Ln^{3+} = Eu^{3+} (**1**) and Tb^{3+} (**3**). Quantum yields of up to 53% (**1**) and 67% (**3**) are remarkable. Obviously, the typical C–H quenching in such compounds is significantly reduced by using a perfluorinated linker. In $^2_\infty[Eu^{III}(tfBDC)(CH_3COO)(FA)_3]\cdot 3FA$ (**7**) (FA = formamide) the quantum yield is reduced to only 10%. This is ascribed to the C–H quenching of the coordinating CH_3COO^- anion. In this respect it seems worthwhile to determine the quantum yields of other Eu^{3+} (ref. 12, 26) and Tb^{3+} (ref. 12, 25) containing coordination polymers with $tfBDC^{2-}$ linkers to investigate the influence of coordinating solvent molecules and additional anions on the luminescence properties in more detail.

In future experiments we are planning to remove DMF in **1** and **3** to obtain compounds with even higher quantum yields. According to DTA/TGA measurements at least two DMF molecules should be removable without decomposing the coordination network. The release of solvent molecules might further lead to compounds with a 3D connected framework. As binuclear units are found in all compounds we have already successfully incorporated two different lanthanide cations in these polymers. Detailed spectroscopic measurements are planned to prove a possible energy transfer between the two lanthanide centers.

Acknowledgements

We thank Dr Ingo Pantenburg and Mr Peter Kliesen for collecting X-ray single crystal data, as well as Mrs Malgorzata Smolarek for DTA/TGA and IR measurements and Mrs Silke Kremer for elemental analysis. The help of Prof. Dr Anja-Verena Mudring and Dr Chantal Lorbeer in recording the first preliminary luminescence spectra and helpful discussions for the interpretation of these data is greatly acknowledged.

Notes and references

1 A. K. Cheetham and C. N. R. Rao, *Science*, 2007, **318**, 58.
2 C. Yang, X. Wang and M. A. Omary, *J. Am. Chem. Soc.*, 2007, **129**, 15454.
3 C. Yang, X. Wang and M. A. Omary, *Angew. Chem., Int. Ed.*, 2009, **48**, 2500.
4 L. Zhang, Q. Wang and Y.-C. Liu, *J. Phys. Chem. B*, 2007, **111**, 4291.
5 Z. Hulvey, D. A. Sava, J. Eckert and A. K. Cheetham, *Inorg. Chem.*, 2011, **50**, 403.
6 P. Pachfule, Y. Chen, J. Jiang and R. Banerjee, *Chem. – Eur. J.*, 2012, **18**, 688.
7 B. Chen, Y. Yang, F. Zapata, G. Qian, Y. Luo, J. Zhang and E. B. Lobkovsky, *Inorg. Chem.*, 2006, **45**, 8882.
8 R. J. Harper, E. J. Soloski and C. Tamborski, *J. Org. Chem.*, 1964, **29**, 2385.

9 A. Orthaber, C. Seidel, F. Belaj, R. Pietschnig and U. Ruschewitz, *Inorg. Chem.*, 2010, **49**, 9350.
10 C. Seidel, R. Ahlers and U. Ruschewitz, *Cryst. Growth Des.*, 2011, **11**, 5053.
11 C. Seidel, C. Lorbeer, J. Cybińska, A.-V. Mudring and U. Ruschewitz, *Inorg. Chem.*, 2012, **51**, 4679.
12 C. M. MacNeill, C. S. Day, A. Marts, A. Lachgar and R. E. Noftle, *Inorg. Chim. Acta*, 2011, **365**, 196.
13 Stoe, *IPDS manual*, Stoe & Cie GmbH, Germany; *X-Red 1.22 Stoe Data Reduction Program*, Stoe & Cie GmbH, Germany, 2001.
14 A. Altomare, G. Cascarano, C. Giacovazzo and A. Gualardi, *J. Appl. Crystallogr.*, 1993, **26**, 343.
15 G. M. Sheldrick, *SHELXL-97: A Program for Crystal Structure Refinement*, University of Göttingen, Germany, 1997, release 97-2; G. M. Sheldrick, *Acta Crystallogr., Sect. A: Fundam. Crystallogr.*, 2008, **64**, 112.
16 *WinGX-Version 1.64.04, An Integrated System of Windows Programs for the Solution, Refinement and Analysis of Single Crystal X-Ray Diffraction Data*, Department of Chemistry, University of Glasgow, UK, 1997–2002; L. J. Farrugia, *J. Appl. Crystallogr.*, 1999, **32**, 837.
17 Crystallographic data (excluding structure factors) for the structures reported in this paper have been deposited at the Cambridge Crystallographic Data Centre as supplementary publication no. CCDC 957999 ($^2_\infty$[Eu(tfBDC)(NO_3)-($DMF)_2$]·DMF, **1**), CCDC 958000 ($^2_\infty$[Gd(tfBDC)(NO_3)-($DMF)_2$]·DMF, **2**), CCDC 958001 ($^2_\infty$[Tb(tfBDC)(NO_3)-($DMF)_2$]·DMF, **3**), CCDC 958002 ($^2_\infty$[Ho(tfBDC)(NO_3)-($DMF)_2$]·DMF, **4**), CCDC 958003 ($^2_\infty$[Tm(tfBDC)(NO_3)-($DMF)_2$]·DMF, **5**), CCDC 1025456 ($^2_\infty$[Sm(tfBDC)(CH_3COO)-$(FA)_3$]·3FA, **6**), CCDC 1025457 ($^2_\infty$[Eu(tfBDC)(CH_3COO)-$(FA)_3$]·3FA, 7), CCDC 1025458 ($^2_\infty$[Ho(tfBDC)(NO_3)$(DMSO)_2$], **8**), CCDC 1025459 ($^2_\infty$[Er(tfBDC)(NO_3)$(DMSO)_2$], **9**), CCDC 1025460 ($^2_\infty$[Tm(tfBDC)(NO_3)$(DMSO)_2$], **10**).
18 *Win XPow, version 3.03*, Stoe & Cie GmbH, Darmstadt, Germany, 2010.
19 (*a*) R. D. Shannon and C. T. Prewitt, *Acta Crystallogr., Sect. B: Struct. Crystallogr. Cryst. Chem.*, 1969, **25**, 925; (*b*) R. D. Shannon, *Acta Crystallogr., Sect. A: Cryst. Phys., Diffr., Theor. Gen. Cryst.*, 1976, **32**, 751.
20 J. V. de Mello, H. F. Wittmann and R. H. Friend, *Adv. Mater.*, 1997, **9**, 230.
21 S. Marks, J. Heck, P. O. Burgos, C. Feldmann and P. W. Roesky, *J. Am. Chem. Soc.*, 2012, **134**, 16983.
22 J. C. Rybak, M. Hailmann, P. R. Matthes, A. Zurawski, J. Heck, C. Feldmann, S. Götzendörfer, J. Meinhardt, G. Sextl, H. Kohlmann, S. Sedlmaier, W. Schnick and K. Müller-Buschbaum, *J. Am. Chem. Soc.*, 2013, **135**, 6896.
23 Z. Hulvey, J. D. Furman, S. A. Turner, M. Tang and A. K. Cheetham, *Cryst. Growth Des.*, 2010, **10**, 2041.
24 Z. Wang, V. C. Kravtsov, R. B. Walsh and M. J. Zaworotko, *Cryst. Growth Des.*, 2007, **7**, 1154.
25 T.-H. Chen, I. Popov, O. Zenasni, O. Daugulis and O. Š. Miljanić, *Chem. Commun.*, 2013, **49**, 6846.
26 S. V. Larionov, L. I. Myachina, L. A. Glinskaya, I. V. Korol'kov, E. M. Uskov, O. V. Antonova, V. M. Karpov, V. E. Platanov and V. P. Fadeeva, *Russ. J. Coord. Chem.*, 2012, **38**, 717.
27 S. V. Larionov, L. I. Myachina, L. A. Sheludyakova, I. V. Korol'kov, O. V. Antonova, V. M. Karpov, V. E. Platanov and V. P. Fadeeva, *Russ. J. Gen. Chem.*, 2014, **84**, 1193.
28 E. A. Mikhalyova, S. V. Kolotilov, M. Zeller, L. K. Thompson, A. W. Addison, V. V. Pavlishchuk and A. D. Hunter, *Dalton Trans.*, 2011, **40**, 10989.